ACS OMEGA

Open Access

http://pubs.acs.org/journal/acsodf

Article

Imidazolium-Based Ionic Liquid-Assisted Silver Nanoparticles and Their Antibacterial Activity: Experimental and Density Functional Theory Studies

Elham Avirdi, Hugues Kamdem Paumo, Boniface Pone Kamdem, Madhur Babu Singh, Kamlesh Kumari, Lebogang Katata-Seru,* and Indra Bahadur*

Cite This: *ACS Omega* 2023, 8, 42976−42986

Read Online

ACCESS | Metrics & More | Article Recommendations

ABSTRACT: The exclusive properties of ionic liquids (ILs) offer various opportunities to develop advanced materials with appreciable therapeutic applications. Imidazolium-based ILs have been frequently used as reaction media and stabilizers for the development and surface functionalization of noble metal nanoparticles (NPs). This study reports the citrate-mediated reduction of silver ions in three different ILs, that is, 1-ethyl-3-methylimidazolium methyl sulfate ([EMIM][MS]), 1-butyl-3-methylimidazolium trifluoromethanesulfonate ([BMIM][OTf]), and 1-butyl-3-methylimidazolium bis(trifluoromethylsulfonyl)-imide ([BMIM][TFSI]). The resulting Ag-ILs NPs were characterized using many analytical techniques, including UV−visible spectroscopy, dynamic light scattering (DLS), scanning electron microscopy, Fourier transform infrared spectroscopy, and X-ray diffraction (XRD). DLS and XRD characterization revealed the negatively charged Ag-[EMIM][MS] NPs, Ag-[BMIM][OTf] NPs, and Ag-[BMIM][TFSI] NPs with mean hydrodynamic sizes of 278, 316, and 279 nm, respectively, and a face-centered cubic structure. These hybrid nanomaterials were subjected to *in vitro* antibacterial screening against three bacterial strains. The Ag-[BMIM][OTf] NPs exhibited significant activities against *Escherichia coli*, *Staphylococcus aureus*, and *Enterobacter cloacae*. The lowest inhibition concentration of 62.5 μg/mL was recorded against *E. coli* using Ag-[EMIM][MS] and Ag-[BMIM][OTf] NPs. Further, the density functional theory calculations carried out on the computed Ag-ILs in the gas phase and water showed relatively stable systems. Ag-[BMIM][TFSI] exhibited the lowest Gibbs free energy change of −34.41 kcal/mol. The value of the global electrophilicity index (ω = 0.1865 eV) for the Ag-[BMIM][OTf] correlated with its good antibacterial activity.

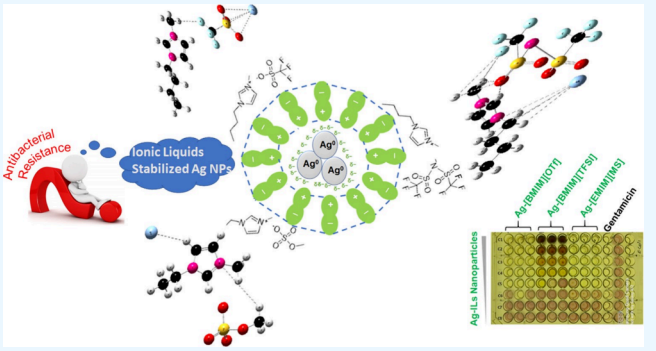

1. INTRODUCTION

Various methods have been reported for synthesizing Ag nanoparticles (NPs), and scientists have systematically been searching for environmentally benign protocols since the "green chemistry" concept in the 1990s.[1−3] Biomass or extracts obtained from different plant species have been widely explored for the reduction of noble metal ions and the stabilization of their corresponding metal NPs.[4−6] At the same time, utilizing ionic liquids (ILs) for the development of noble metal NPs has also emerged as a green route.[7,8] ILs consisting of anions and bulky organic cations demonstrate important characteristics, such as negligible volatility, good ionic conductivity, and high thermal stability. These liquid salts are identified as designer solvents since their properties can be tailored by varying the anion−cation combination. Because of the electrostatic interactions, hydrogen bonding, and van der Waals forces, ILs can achieve not only a relatively high nucleation rate of metallic NPs but also their electronic and steric stabilization.

Ag NPs have continued to draw a lot of interest from the scientific community owing to their inhibition effects toward a variety of pathogenic microorganisms.[9,10] These properties depend greatly on their physical characteristics, such as particle size, surface charge, and coating. Fourier transform infrared (FTIR), nuclear magnetic resonance (NMR), and surface-enhanced Raman spectroscopy suggested that the antipathogenic activities of Ag NPs arise from the decomposition of

Received: August 20, 2023
Accepted: September 13, 2023
Published: November 2, 2023

purine-related metabolites by the NPs and/or their released Ag^+ ions.[11] Nevertheless, bacterial tolerance and resistance to Ag NPs and Ag^+ ions have been discussed previously.[12] This may be attributed to the extracellular polymers secreted by numerous microorganisms or the reduced dissolution of the Ag^+ ions. The ever-growing issue about multidrug-resistant bacteria in recent years has become an urgent public health crisis worldwide.[13,14]

Numerous research papers have raised concerns about the aggregation-prone characteristics of Ag NPs during the colloidal synthesis in aqueous solutions as well as their unstability in biological media.[15] ILs as synthesis media can provide physical and chemical protection to the developing NPs, thereby improving their stability and the efficacy of the resulted nanomaterials. It is worth noting that specific structural features and biological activities of noble metal NPs are every so often ascribed to coating agents on their surface.[16] It has been established that surface active ILs can disrupt cellular structure and facilitate uptake of NPs and their solutes into cells.[17,18] Moreover, variations in the molecular structure of the anions or cations may alter the properties of ILs and influence the antibacterial potential of the coated noble metal NPs.[19] On account of their unique properties, ILs have provided valuable opportunities for the development of novel active pharmaceutical ingredients. Earlier studies revealed that these can play an important role in preserving or optimizing the efficacy of antibacterial drugs and prodrugs.[20−22]

Limited experimental and theoretical studies have taken up the property enhancement of IL-stabilized Ag NPs for antimicrobial solicitation.[23] New approaches for the discovery of antibacterial drugs are paramount to our efforts in the continuing fight against multidrug-resistant bacteria. Earlier, we reported the cation effects of 1-ethyl-3-methylimidazolium tetrafluoroborate ([EMIM][BF_4]) and 1-butyl-3-methylimidazolium tetrafluoroborate ([BMIM][BF_4]) on the synthesis of stable and biologically active Ag NPs (132 and 360 nm).[24] The chemical reduction of Ag^+ ions in [BMIM][BF_4] afforded larger NPs with promising activities against Gram-negative (G−ve) *Escherichia coli* and *Enterobacter cloacae* and Gram-positive (G+ve) *Staphylococcus aureus*. This work investigates the substituent effects of three other ILs, namely, [EMIM][MS], [BMIM][OTf], and [BMIM][TFSI] (Figure 1), on the synthesis of Ag NPs. The physicochemical properties of the developed Ag-ILs NPs were examined, and their antimicrobial activities were evaluated against *E. coli* ATCC 25922, *E. cloacae* ATCC 700323, and *S. aureus* ATCC 25923. Density functional theory (DFT) computations on the Ag-ILs systems were completed in the gas phase and water to elucidate the electronic and thermodynamic properties of the synthesized nanomaterials, which might influence the antibacterial activities.

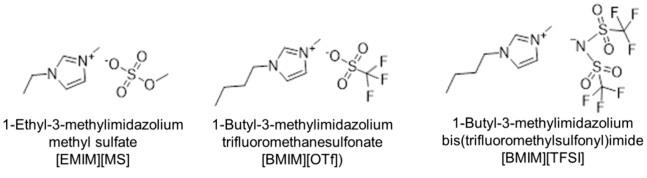

Figure 1. Molecular structures of the ILs [EMIM][MS], [BMIM][OTf], and [BMIM][TFSI].

2. EXPERIMENTAL SECTION

2.1. Synthesis of the Ag-ILs NPs. Sodium citrate ($Na_3C_6H_5O_7$), silver nitrate ($AgNO_3$), and ILs [EMIM][MS], [BMIM][OTf], and [BMIM][TFSI] were acquired from Sigma-Aldrich (JHB, South Africa). Ag^+ ions were reduced in the presence of citrate ions in [EMIM][MS], [BMIM][OTf], and [BMIM][TFSI] to generate Ag-[EMIM][MS] NPs, Ag-[BMIM][OTf] NPs, and Ag-[BMIM][TFSI] NPs, respectively. The citrate ions acted as a strong chelating agent and a mild reductant.[25] In brief, $Na_3C_6H_5O_7$ (0.14 g, 0.85 mmol) in 30 mL of [EMIM][MS] and $AgNO_3$ (0.22 g, 0.85 mmol) in 30 mL of [EMIM][MS] were stirred at 80 °C for 48 h and then allowed to cool to room temperature. Next, the citrate solution was added dropwise to the stirred silver solution at 40 °C, and stirring was continued for 4 h. Subsequently, the pH of the reaction milieu was adjusted to 8.0 and the colloidal solution was centrifuged for 1 h to isolate the Ag-[EMIM][MS] NPs. Similarly, the Ag-[BMIM][OTf] NPs and Ag-[BMIM][TFSI] NPs were developed. All nanomaterials in this work were freeze-dried and stored at room temperature.

2.2. Characterization of the Ag-ILs NPs. In this work, we have tried to study the physicochemical attributes of the Ag-ILs NPs with various characterization techniques. These included UV−vis spectroscopy on a PerkinElmer UV/vis Lambda 365 instrument, DLS (for measuring the hydrodynamic size, polydispersity index, and ζ-potential) using a Malvern Zetasizer Nano ZS-90, SEM on a Zeiss Crossbeam 540 FEG-SEM microscope, FTIR spectroscopy on a PerkinElmer spectrum 100 spectrophotometer, and X-ray diffraction (XRD) on a Bruker Advance-D8 diffractometer using Cu K_α radiation.

2.3. Evaluation of the Antibacterial Activities of the Ag-ILs NPs. The antibacterial activities of the Ag-ILs NPs were determined against three bacterial pathogens obtained from the American Type Culture Collection (ATCC) standard: *E. coli* ATCC 25922, *S. aureus* ATCC 25923, and *E. cloacae* ATCC 700323. The bacterial strains were subcultured on tryptic-soy agar plates for 18 h at 37 °C. Luria−Bertani broth (10 mL) was inoculated with each colony and then was incubated at 37 °C for 18 h with continuous shaking at 120 rpm. To collect bacterial cells in the log phase, 100 μL of the overnight broth culture was subcultured for 3 h at 37 °C in 10 mL of Luria−Bertani broth. The bacterial culture was then calibrated to the 0.5 McFarland standard: equivalent to 1×10^8 CFU/mL.

2.3.1. Determination of Minimal Inhibitory Concentration (MIC). As indicated in the CLSI (Clinical and Laboratory Standards Institute) laboratory manual M49-A,[26] the MICs were determined by the microplate dilution method. In this process, different concentrations of Ag-ILs NPs and gentamicin (positive control) were used. In brief, solutions of Ag-[EMIM][MS] NPs, Ag-[BMIM][OTf] NPs, and Ag-[BMIM][TFSI] NPs were prepared under aseptic conditions in sterile distilled water to a concentration of 4 mg/mL. After which, 100 μL of each solution was serially diluted 2-fold in Mueller−Hinton broth using a 96-well round-bottom microtiter plate to obtain final concentrations ranging from 0.0079 to 1000 μg/mL. Similarly, gentamicin (Gibco), the positive control, was 2-fold serially diluted for each bacterium to final concentrations ranging from 0.039 to 50 μg/mL. Bacterial suspension (100 μL), standardized to McFarland standard no.

https://doi.org/10.1021/acsomega.3c06171
ACS Omega 2023, 8, 42976−42986

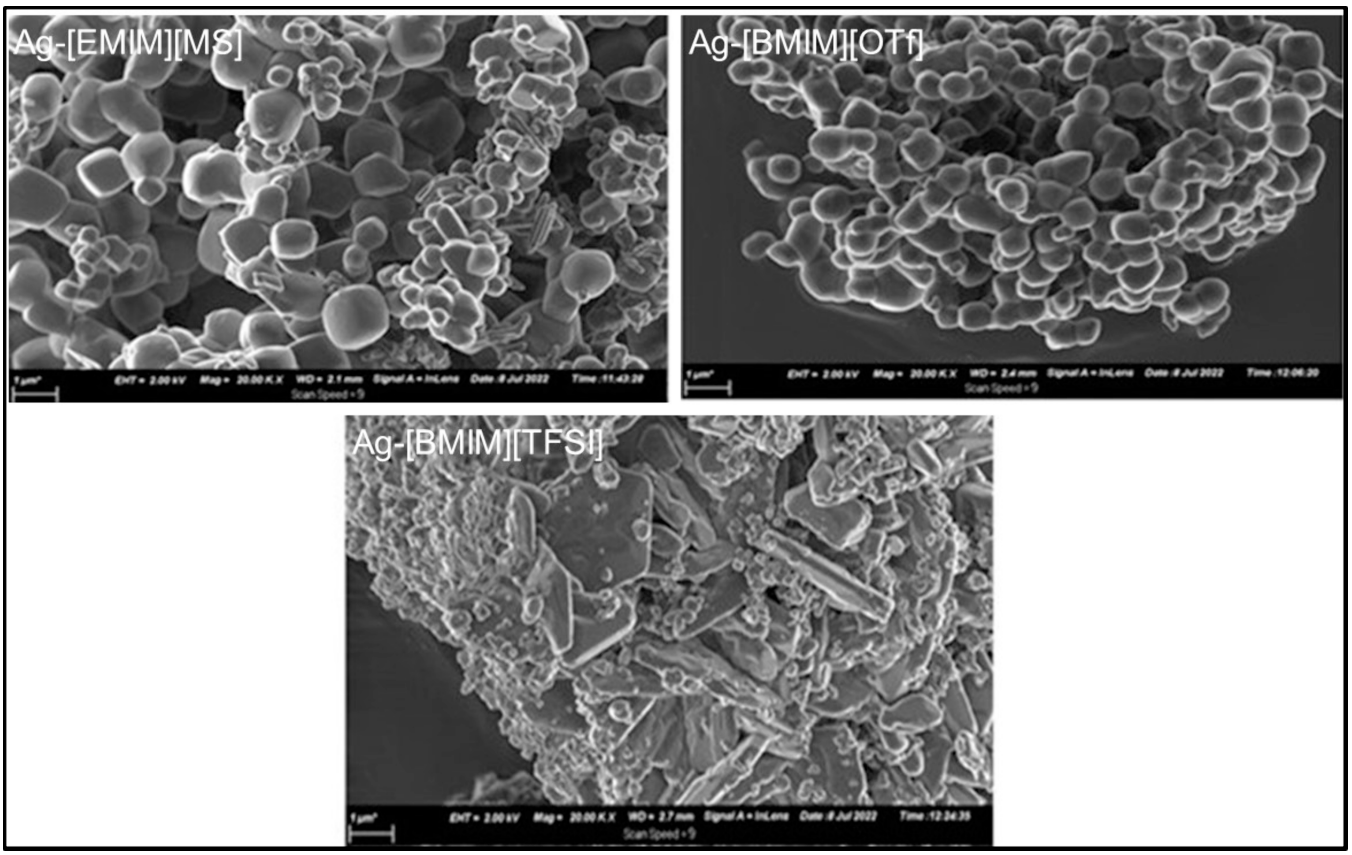

Figure 2. SEM micrographs of the Ag-ILs NPs.

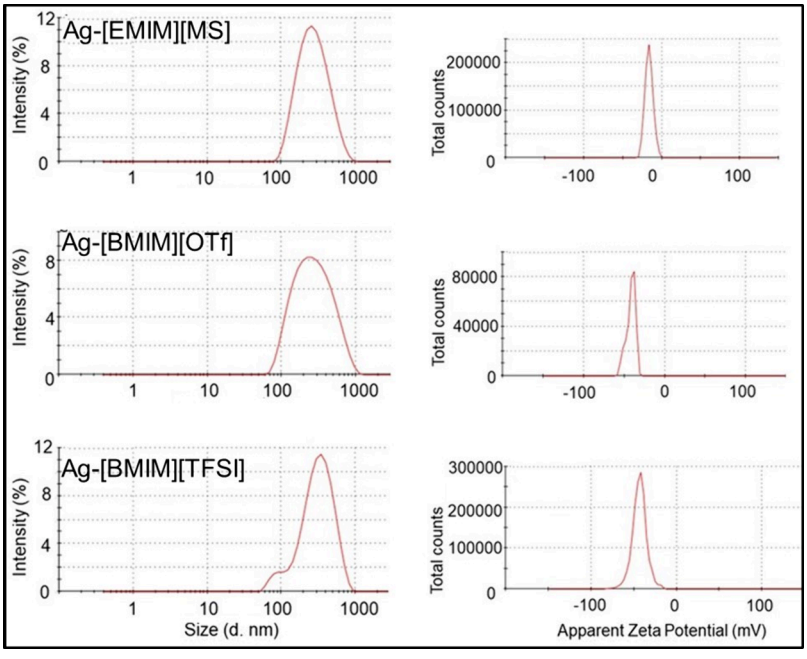

Figure 3. Hydrodynamic size and apparent ζ-potential of Ag-ILs NPs.

0.5, was added to each well. Plates were sealed and incubated at 37 °C for 24 h. To indicate growth, 40 μL of *p*-iodonitrotetrazolium violet (INT) (Sigma-Aldrich) was added to each well. Plates were resealed and incubated at 37 °C for 30−45 min for color development. The presence of bacterial growth was indicated by a pink/purple color, and clear wells indicated the inhibition of bacterial growth. The assay was performed in triplicate and repeated twice.

2.3.2. Determination of Minimal Bactericidal Concentration (MBC). The dilution in the broth method was used to calculate the MBC for the antibacterial agents.[26] This parameter was recorded as the lowest concentration of the

https://doi.org/10.1021/acsomega.3c06171
ACS Omega 2023, 8, 42976−42986

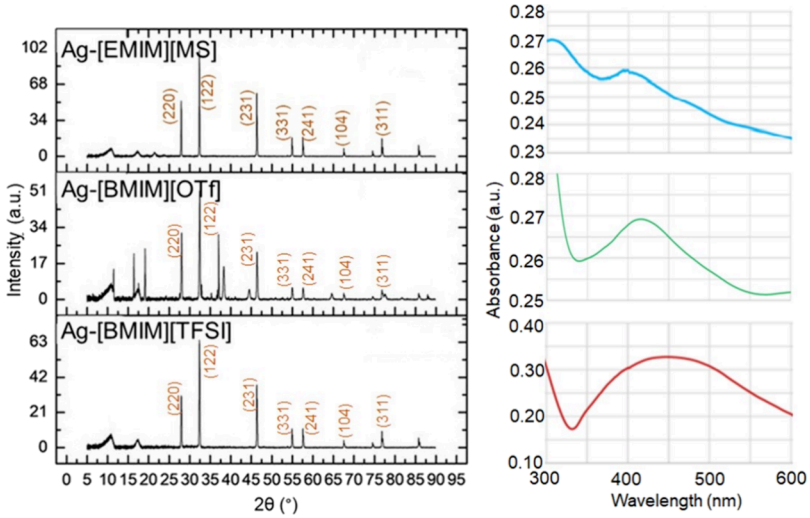

Figure 4. XRD patterns and UV−vis spectra of Ag-ILs NPs.

Ag-ILs NPs and gentamicin that can eliminate 100% growth of the test organisms under the experimental conditions. In brief, 50 μL aliquots of the preparations that did not show any visible growth after incubation during the MIC assay were added to 50 μL of INT to 100 μL of Mueller−Hinton broth. Next, the plates were incubated at 37 °C for 24 h. The presence of bacterial growth was indicated by a pink/red color, and clear wells indicated the inhibition of bacterial growth. The lowest concentration that indicated inhibition of growth was recorded as MBC.

2.4. DFT Computations. The structures of all the ILs and Ag-ILs were drawn using ChemDraw Professional 15.0, and minimization of structure energy was done with Chem3D by applying MM2.[27,28] DFT calculation has been performed to comprehend the thermodynamic properties and the delocalization of the electron density on chemical entities. It provides various frontier molecular orbitals, optimization energies, free energies, and other energies to chemical entities. All the calculations were performed by using the Gaussian 16 software to apply the DFT/B3LYP model and LanL2DZ basic set.[29−31] Different thermodynamic parameters of the ILs and Ag-ILs were calculated in default and water, and the results were extracted by GaussView 6.[32]

3. RESULTS AND DISCUSSION

3.1. SEM and DLS Measurements. The morphology of the silver NP products was found to be dependent on the chemical structure of the ILs. The SEM images of Ag-[EMIM][MS] NPs and Ag-[BMIM][OTf] NPs exhibited well-defined cubic shapes (Figure 2). On the other hand, the morphological structure of the Ag-[BMIM][TFSI] NPs was characterized by small quasi-spherical shapes and large plates. A previous report by Kim and co-workers described the formation of silver nanowires in 1-butyl-3-methylimidazolium coupled with methyl sulfate [BMIM][MS].[33]

The mean hydrodynamic sizes for the prepared Ag-[EMIM][MS] NPs, Ag-[BMIM][OTf] NPs, and Ag-[BMIM]-[TFSI] NPs were 278, 316, and 279 nm, respectively, with polydispersity index values between 0.34 and 0.39 (Figure 3). As compared with the Ag-[BMIM][OTf] NPs, the Ag-[BMIM][TFSI] NPs with a higher fluorine content displayed a smaller particle size in accordance with the previous literature.[34] The ζ-potential values for these silver NPs at various ILs were negative in the range of −20 to −43 mV. These suggest the electrostatic repulsion and stability of the Ag-ILs NPs in water. The charged ion aggregates of [EMIM][MS], [BMIM][OTf], and [BMIM][TFSI] form electrical double-layer structures on the surface of the developing Ag NPs, thus ensuring their colloidal stabilization.[35] The magnitude of the ζ-potential value determines the extent of repulsion of the NPs in the dispersion medium. The reported ζ-potential indicates a noteworthy shift toward less negative values for the Ag-[BMIM][OTf] and Ag-[BMIM]-[TFSI] NPs. This may occur because of the long alkyl chain of the $BMIM^+$ cation and the fluoroalkyl group of the anions, which provide hydrophobicity and amplify the electrostatic character.[36] Due to the high electronegativity of fluorine, the C−F bonds of OTf^- and $TFSI^-$ anions are polarized.

3.2. UV−Vis Absorption and XRD. The UV−vis absorption spectra of the nanomaterials dispersed in water were recorded, and these exhibited maximum absorption bands in the range of 350−450 nm (Figure 4). The collective oscillation of electron plasmon and their interaction with incident electromagnetic radiation causes a surface plasmon band in the UV−vis domain.[37] In this light, the results obtained for the Ag-[EMIM][MS] NPs, Ag-[BMIM][OTf] NPs, and Ag-[BMIM][TFSI] NPs suggest that plasmonic silver NPs were generated. Moreover, as the particle size increased significantly in [BMIM][TFSI], the plasmon band of the Ag-[BMIM][TFSI] NPs broadened.

The crystallization behavior was also studied through the acquired XRD patterns (Figure 4). The three types of Ag-ILs NPs displayed representative peaks at 2θ 27.6, 32.1, 46.5, 55.0, 57.6, 67.8, and 76.9°, which were assigned to (220), (122), (231), (331), (241), (104), and (311) diffractions of silver, respectively. These results demonstrated that the Ag NPs obtained in this study were crystallized in a face-centered cubic structure.[38]

3.3. FTIR. The Ag-ILs NPs were analyzed by FTIR spectroscopy in the range of 400−4000 cm^{-1} to show the coating and stabilization of silver NPs during the interaction with ILs. The FTIR spectra recorded are shown in Figure 5. All of the Ag-ILs NPs exhibited a broad feature in the range of 2100−3600 cm^{-1} attributable to hydrogen bonding between anions and cations of the ILs. The weak transmittance peaks

https://doi.org/10.1021/acsomega.3c06171
ACS Omega 2023, 8, 42976−42986

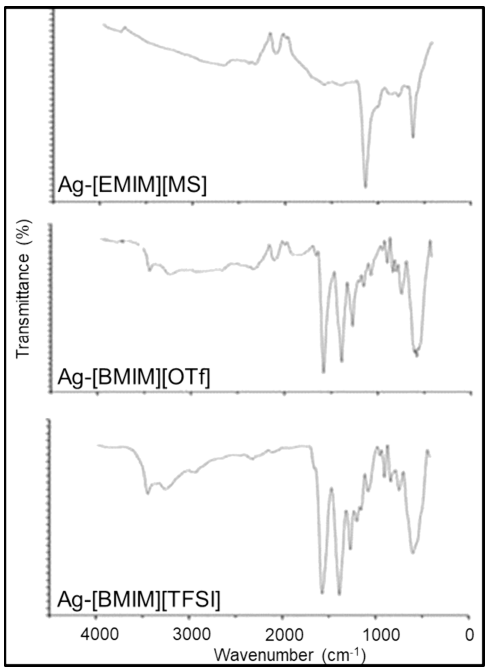

Figure 5. FTIR spectra of Ag-ILs NPs.

observed in this region were ascribed to the C−H asymmetric and symmetric stretching of the alkyl tail on the imidazolium cations.[39] The sharp peaks located in the range of 550−850 cm^{-1} were due to out-of-plane bending of the imidazole ring and its aromatic C−H. The strong peak at ∼1095 cm^{-1} in the spectrum of the Ag-[EMIM][MS] NPs was assigned to the imidazolium in-plane ring bending vibration. The S−O/S=O bond vibration was observed in the 1050−1250 cm^{-1} spectral range,[40] while evidence for the C−F asymmetrical and symmetrical stretch of OTf^- and $TFSI^-$ was provided with the presence of intense and sharp peaks at ∼1354 and ∼1592 cm^{-1}, respectively. As compared to neat [BMIM][OTf] and [BMIM][TFSI],[39,41] the corresponding IL-stabilized Ag NPs demonstrated a shift of C−F transmittance peaks toward higher frequencies. This was attributed to hydrogen bonds between the C(2)−H of the imidazolium ring and the C−F of the OTf^- and $TFSI^-$ anions. It is noteworthy that hydrogen bonds can also form between C(2)−H of the imidazolium ring and S=O of the MS^-, OTf^-, and $TFSI^-$ anions.

3.7. Antibacterial Activity. Table 1 presents the MIC and MBC values of the Ag-ILs NPs and gentamicin. The

Table 1. Recorded MIC and MBC Values of the Ag-ILs NPs

	MIC and MBC (μg/mL)					
	E. coli		*S. aureus*		*E. cloacae*	
Ag-ILs NPs	MIC	MBC	MIC	MBC	MIC	MBC
Ag-[EMIM][MS] NPs	62.5	62.5	500	500	250	250
Ag-[BMIM][OTf] NPs	62.5	125	125	125	125	500
Ag-[BMIM][TFSI] NPs	125	125	125	125	125	250
gentamicin	0.78		0.78		3.13	

fluorinated Ag-[BMIM][OTf] NPs and Ag-[BMIM][TFSI] NPs demonstrated moderate antibacterial activities against *S. aureus* and *E. cloacae* with a common MIC value of 125 μg/mL vs gentamicin (MIC: 0.78 and 3.13 μg/mL against *S. aureus* and *E. cloacae*, respectively). Against *E. cloacae* and *S. aureus*, the Ag-[EMIM][MS] NPs were considered poorly active, as this nanomaterial displayed MIC values of 250 and 500 μg/mL, respectively. The Ag-[EMIM][MS] NPs and Ag-[BMIM]-[OTf] NPs inhibited the growth of *E. coli* with a common MIC value of 62.5 μg/mL vs gentamicin (MIC: 0.78 μg/mL). The Ag-[EMIM][MS] NPs exhibited MBC values of 62.5, 250, and 500 μg/mL in *E. coli*, *E. cloacae*, and *S. aureus*, respectively, whereas the Ag-[BMIM][OTf] NPs and Ag-[BMIM][TFSI] NPs afforded a common MBC value of 125 μg/mL when tested against *E. coli* and *S. aureus*. It has been argued through the structure−activity relationships that components of ILs can play a key role in the antibacterial properties of IL-stabilized noble metal NPs.[42−44] Fluorine substitution may improve the solubility and bioavailability of [BMIM][OTf] and [BMIM]-[TFSI] coatings. Earlier investigations demonstrated that imidazolium-containing ILs could show an inhibitory effect on the growth of *E. coli* and *S. aureus*.[42] Furthermore, the greater repulsion between the Ag-[BMIM][OTf] NPs and Ag-[BMIM][TFSI] NPs, as seen from DLS measurements, may account for their pronounced antibacterial activities against *E. coli*, *S. aureus*, and *E. cloacae*. Even though studies of IL microbial susceptibility have been performed in the literature, most of these have shown that the MIC value against *E. coli* is greater than that of *S. aureus*.[42] By contrast, the results obtained in this study suggest that the inhibitory and potential antibacterial mode of action is not attributable to the selected ILs but instead the presence of Ag NPs stabilized by IL layers. The values of MIC for *S. aureus* were higher than those obtained for *E. coli*. This outcome is unexpected because *E. coli* is a G−ve bacterium with a lipopolysaccharide-containing outer membrane less susceptible to antimicrobial agents' penetration, as compared to G+ve *S. aureus*.[45,46] Conversely, Ahmad et al.[47] and More et al.[48] have demonstrated that the thinner peptidoglycan cell wall of G−ve bacteria is more liable to Ag NPs than their G+ve counterparts. The later possess a thick peptidoglycan layer that can act as a barrier for the cell penetration of Ag NPs and their released Ag^+ ions.[49] The antibacterial activities of Ag-ILs NPs may include (i) release of Ag NPs and Ag^+ ions, (ii) adhesion of the released components to the cytoplasmic membrane, (iii) uptake of the free Ag NPs and Ag^+ ions by the cells, and (iv) generation of free radicals and modulation of cell signaling pathways.[50]

Vibrational spectroscopy of the Ag NPs in 1-butyl-3-methylimidazolium tetrafluoroborate ([BMIM][BF_4]) has revealed the electric double-layer characteristics of ILs in which the cations (positively charged layer) have more interactions with the metal surface.[51] Additionally, NMR spectroscopy has suggested that the imidazolium ring reacts with the metal nanoclusters transiently to build surface-attached carbenes.[52] Hence, the structural organization of the developed Ag-ILs NPs could also influence their performances. It has been reported that the Ag NPs in 1-butyl-3-methylimidazolium methanesulfonate ([BMIM][MS]) displayed larger diameters of inhibition against *E. coli* and *S. aureus* strains at a higher dose (2000 μg/mL).[53]

Overall, this study demonstrates the *in vitro* antibacterial potency of the ILs ([EMIM][MS], [BMIM][OTf], and [BMIM][TFSI]) surface-functionalized Ag NPs and can serve as a basis for the development of promising antibacterial agents to fight against the problem of microbial drug resistance. However, toxicity experiments and pharmacokinetics should be considered for the successful application of IL-stabilized Ag NPs in medicine.

https://doi.org/10.1021/acsomega.3c06171
ACS Omega 2023, 8, 42976−42986

3.8. DFT. The frontier molecular orbitals and their energies are useful characteristics for predicting the charge transfer within a compound and assessing its reactivity.[54] The HOMO and LUMO surfaces of the [EMIM][MS], Ag-[EMIM][MS], [BMIM][OTf], Ag-[BMIM][OTf], [BMIM][TFSI], and Ag-[BMIM][TFSI] in the default and water systems are shown in Figure 6. The HOMO levels consisted of orbitals from the imidazolium ring for the neat ILs. But after the introduction of Ag, the charge density localization shifted toward the anions of the ILs. The Ag-[EMIM][MS], Ag-[BMIM][OTf], and Ag-[BMIM][TFSI] had HOMO−LUMO energy gaps (E_L−E_H) of 0.0914, 0.18827, and 0.08052 eV in the gaseous state and 0.18035, 0.18817, and 0.14113 eV in water, respectively (Table 2). A low value of energy gap is associated with antiaromaticity and high reactivity in chemical processes.[55] The minimum energy gap was recorded with Ag-[BMIM][TFSI] in the gaseous state and water.

Various physicochemical descriptors were also calculated in default and water systems, and these included the hardness (η), softness (S), absolute electronegativity (χ), chemical potential (μ), and global electrophilicity index (ω) (Table 2). The hardness values for the neat ILs were greater than those calculated for their corresponding Ag-integrated derivatives. Thus, the later were considered more reactive[56] and the order of reactivity was Ag-[BMIM][TFSI] > Ag-[EMIM][MS] > Ag-[BMIM][OTf]. On the other hand, the electronegativity values increased in the order Ag-[EMIM][MS] < Ag-[BMIM][OTf] < Ag-[BMIM][TFSI]. One of the most important quantum chemical descriptors, the electrophilicity index, evaluates compounds' reactivity and site selectivity to determine toxicity and assessing the biological activity.[57] The global electrophilicity index estimates the amount of energy lost due to maximal electron transfer between the donor and the acceptor, as shown by HOMO−LUMO energy values. This parameter was used to compare the electrophilic nature of the Ag-ILs systems. The order of the reactivity index was found to be Ag-[BMIM][TFSI] > Ag-[EMIM][MS] > Ag-[BMIM][OTf]. The result was best correlated with the biological activities of the synthesized Ag-ILs NPs. Marinescu et al. reported an increase in the antimicrobial activity of benzimidazole-based compounds with a decreasing value of ω.[58]

The thermodynamic properties of the neat ILs and IL-stabilized Ag were also predicted in the default and water system by the DFT approach. The zero-point energies, thermal energies, thermal enthalpies, thermal free energies, optimization energies, and dipole moments for the [EMIM][MS], Ag-[EMIM][MS], [BMIM][OTf], Ag-[BMIM][OTf], [BMIM]-[TFSI], and Ag-[BMIM][TFSI] are given in Table 3. The thermal free energies for the [EMIM][MS], [BMIM][OTf], and [BMIM][TFSI] were determined to be −695.235525, −996.338696, and −1473.787974 hartree/particle in default and −695.235554, −996.338649, and −1473.787741 hartree/particle in water, respectively. After introducing Ag, the thermal free energies of −841.227267, −1142.290925, and −1619.776755 hartree/particle in default and −841.006988, −1142.108287, and −1619.776195 hartree/particle in water were recorded. These values indicate a decrease in the thermal free energy after the introduction of Ag in ILs. Ag-[BMIM][TFSI] showed the minimum thermal free energy in both the default and water. Geometry optimization performed by DFT methods provides the most stable structure on the basis of the lowest possible ground state energy. The optimization energies for the [EMIM][MS], [BMIM][OTf], and [BMIM][TFSI] were computed to be −695.408422, −996.530371, and −1473.987740 hartree/particle in default and −695.408421, −996.530371, and −1473.987922 hartree/

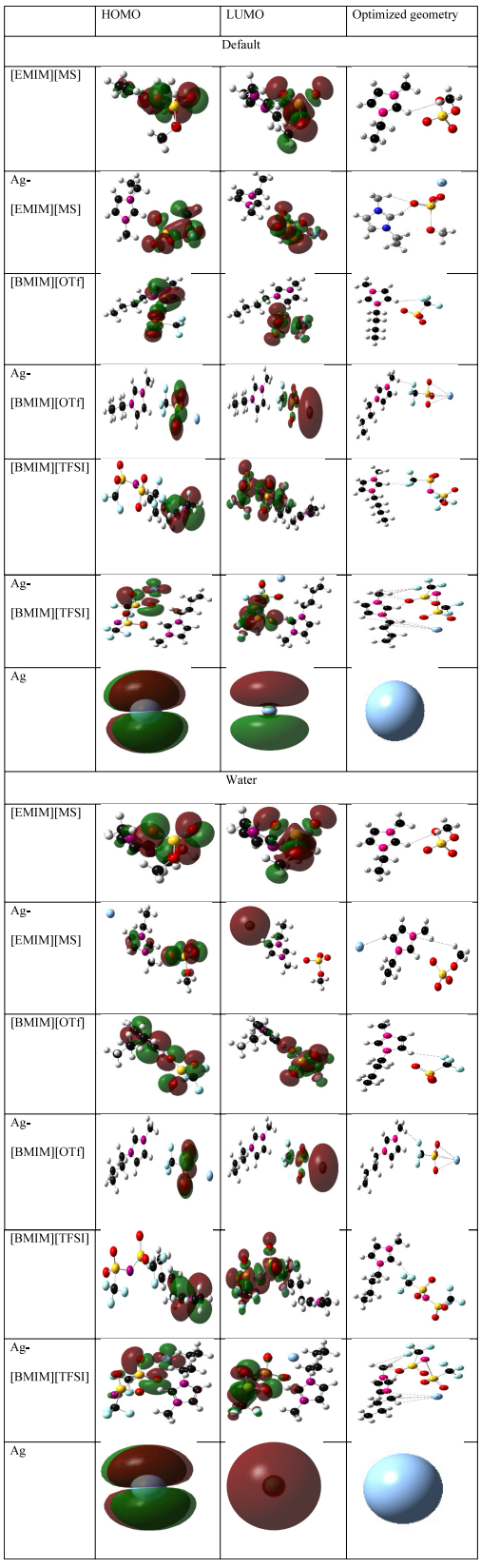

Figure 6. HOMO, LUMO, and optimized geometry for the neat ILs and Ag-ILs in the default and water system.

https://doi.org/10.1021/acsomega.3c06171
ACS Omega 2023, 8, 42976−42986

Table 2. Quantum Chemical Descriptors for the Neat ILs and Ag-ILs in the Default and Water System

compound	E_H (eV)	E_L (eV)	E_L-E_H (eV)	E_L+E_H (eV)	η (eV)	χ (eV)	S (eV)	μ (eV)	ω (eV)
Gaseous State									
[EMIM][MS]	−0.27899	−0.06880	0.21019	−0.34779	0.105095	0.173895	4.7576003	−0.17389	0.1438673
Ag-[EMIM][MS]	−0.21902	−0.12762	0.0914	−0.34664	0.0457	0.17332	10.940919	−0.17332	0.3286633
[BMIM][OTf]	−0.28264	−0.07287	0.20977	−0.35551	0.104885	0.177755	4.7671259	−0.17775	0.1506261
Ag-[BMIM][OTf]	−0.28153	−0.09326	0.18827	−0.37479	0.094135	0.187395	5.3115207	−0.18739	0.1865241
[BMIM][TFSI]	−0.29	−0.11959	0.17041	−0.40959	0.085205	0.204795	5.8682002	−0.20479	0.2461181
Ag-[BMIM][TFSI]	−0.26297	−0.18245	0.08052	−0.44542	0.04026	0.22271	12.419275	−0.22271	0.6159928
Ag	−0.29227	−0.00539	0.28688	−0.29766	0.14344	0.14883	3.485778	−0.14883	0.0772113
Water									
[EMIM][MS]	−0.27899	−0.06879	0.2102	−0.34778	0.1051	0.17389	4.7573739	−0.17389	0.1438522
Ag-[EMIM][MS]	−0.27665	−0.0963	0.18035	−0.37295	0.090175	0.186475	5.5447741	−0.18647	0.192808
[BMIM][OTf]	−0.28264	−0.07288	0.20976	−0.35552	0.10488	0.17776	4.7673532	−0.17776	0.1506418
Ag-[BMIM][OTf]	−0.28142	−0.09325	0.18817	−0.37467	0.094085	0.187335	5.3143434	−0.18733	0.1865037
[BMIM][TFSI]	−0.29028	−0.1196	0.17068	−0.40988	0.08534	0.20494	5.8589173	−0.20494	0.2460769
Ag-[BMIM][TFSI]	−0.26073	−0.1196	0.14113	−0.38033	0.070565	0.190165	7.0856657	−0.19016	0.256237
Ag	−0.29227	−0.0927	0.19957	−0.38497	0.099785	0.192485	5.0107732	−0.19248	0.1856515

Table 3. Thermodynamic Parameters for the Neat ILs and Ag-ILs in the Default and Water System

structure	zero-point energies (hartree/particle)	thermal energies (hartree/particle)	thermal enthalpies (hartree/particle)	thermal free energies (hartree/particle)	optimization (hartree/particle)	dipole moments (debye)
Default						
Ag-[EMIM][MS]	−841.01	−840.98	−840.98	−841.06	−841.22	13.97
[EMIM][MS]	−695.18	−695.16	−695.16	−695.23	−695.41	21.51
Ag-[BMIM][OTf]	−1142.04	−1142.01	−1142.01	−1142.10	−1142.29	36.71
[BMIM][OTf]	−996.28	−996.25	−996.25	−996.33	−996.53	27.10
Ag-[BMIM][TFSI]	−1619.70	−1619.66	−1619.66	−1619.77	−1619.97	25.85
[BMIM][TFSI]	−1473.71	−1473.68	−1473.68	−1473.78	−1473.98	37.72
Ag	−145.76	−145.75	−145.75	−145.77	−145.76	00
Water						
Ag-[EMIM][MS]	−840.94	−840.92	−840.92	−841.01	−841.17	22.53
[EMIM][MS]	−695.18	−695.16	−695.16	−695.23	−695.41	21.51
Ag-[BMIM][OTf]	−1142.04	−1142.01	−1142.01	−1142.10	−1142.28	39.46
[BMIM][OTf]	−996.28	−996.25	−996.25	−996.33	−996.53	27.11
Ag-[BMIM][TFSI]	−1619.69	−1619.66	−1619.66	−1619.77	−1619.96	27.36
[BMIM][TFSI]	−1473.71	−1473.68	−1473.68	−1473.78	−1473.98	38.03
Ag	−145.76	−145.75	−145.75	−145.77	−145.76	00

particle in water, respectively. As for the Ag-[EMIM][MS], Ag-[BMIM][OTf], and Ag-[BMIM][TFSI], the optimization energies were −841.227267, −1142.290925, and −1619.970363 hartree/particle in default and −695.408421, −1142.289568, and −1619.968255 hartree/particle in water, respectively. A comparison of the optimized geometries of Ag-ILs showed the formation of imidazolium C−H•••Ag bonds for the Ag-[EMIM][MS] and Ag-[BMIM][TFSI]. The OTf^- S=O−/O=S−Ag bridges were observed for the Ag-[BMIM]-[OTf]. These findings suggest that the [EMIM][MS] and [BMIM][TFSI] form complexes with Ag NPs by cation interactions to the surface, while the [BMIM][OTf] is distributed over the NP surface by anion coordination.

The dipole moment is an important parameter that gives information about the polarity and solubility of compounds. Among the ILs selected for this investigation, [BMIM][TFSI] exhibited superior dipole moment in default (37.72 D) and water (38.03 D) (Figure 7a). After the addition of Ag, a rapid change in dipole moment was observed, and Ag-[BMIM]-[OTf] was found to display maximum values in default (36.71 D) and water (39.47 D) (Figure 7b). This indicates that the most potent Ag-[BMIM][OTf] NPs can release Ag NPs or Ag^+ ions with ease in the biological medium and may explain its higher inhibitory effect against *E. coli* and broader spectrum of activity. Ag^+ ions play a major role in killing bacteria owing to their ability to interact with most biomolecules (DNA,

https://doi.org/10.1021/acsomega.3c06171
ACS Omega 2023, 8, 42976−42986

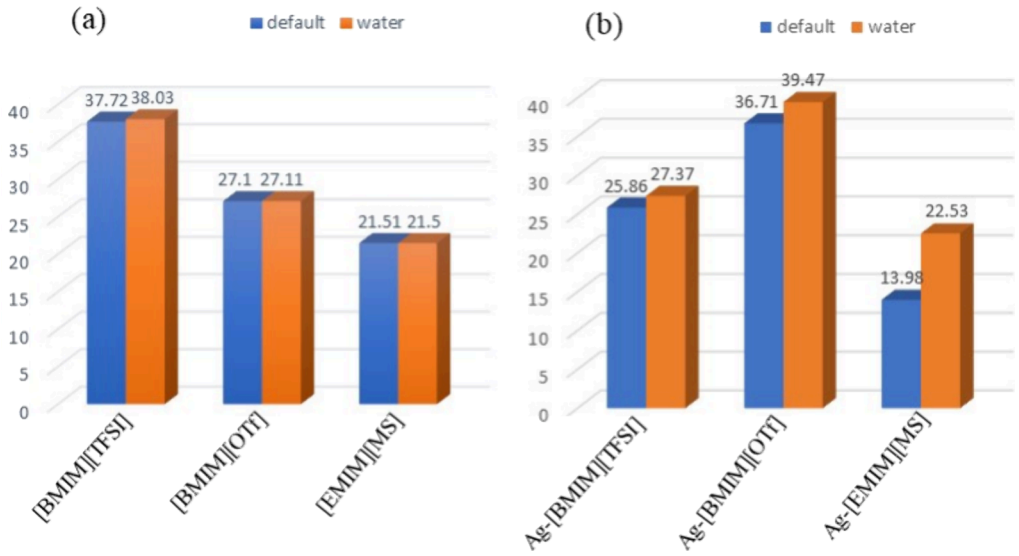

Figure 7. Dipole moments for the (a) neat ILs and (b) Ag-ILs in the default and water system.

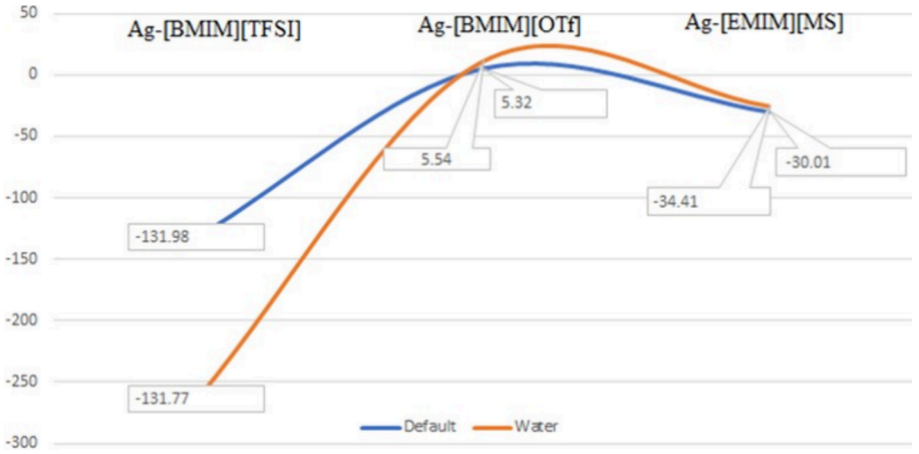

Figure 8. ΔG_f (kcal/mol) for the formation of Ag-ILs in default and water.

membrane proteins, enzymes, or intracellular cofactors) and disrupt cellular processes.[59]

Theoretically, the stabilization of Ag by ILs can be evaluated by determining the change in the Gibbs free energy ΔG_f. The computed ΔG_f for the Ag-[EMIM][MS], Ag-[BMIM][OTf], and Ag-[BMIM][TFSI] were −131.98, 5.32, and −30.01 kcal/mol in default and −137.77, 5.54, and −34.41 kcal/mol in water (Figure 8). These results indicate that the formation of the proposed Ag-ILs is more feasible in default as compared to the water system. Moreover, the negative value of ΔG_f, calculated for Ag-[EMIM][MS] and Ag-[BMIM][TFSI], suggests that the stabilizing processes for silver by [EMIM]-[MS] and [BMIM][TFSI] is spontaneous. On the other hand, the positive value for the Ag-[BMIM][OTf] system indicates nonspontaneous developments.

4. CONCLUDING REMARKS

The development of Ag NPs stabilized by 1-ethyl-3-methylimidazolium methyl sulfate ([EMIM][MS]), 1-butyl-3-methylimidazolium trifluoromethanesulfonate ([BMIM]-[OTf]), and 1-butyl-3-methylimidazolium bis-(trifluoromethylsulfonyl)imide ([BMIM][TFSI]) was confirmed by XRD and FTIR analyses. It was observed that these NPs had spherical-like and nonspherical shapes depending upon the IL used for their preparation. The Ag-[BMIM][TFSI] NPs and Ag-[BMIM][OTf] NPs demonstrated moderate antibacterial activity (MIC: 125 μg/mL) against *S. aureus* and *E. cloacae*. The two most potent nanomaterials (Ag-[EMIM][MS] NPs and Ag-[BMIM][OTf] NPs) inhibited the growth of *E. coli* with a common MIC value (62.5 μg/mL). DFT calculations of the Ag-ILs systems suggested that Ag NPs undergo interactions with the cationic ($EMIM^+$ and $BMIM^+$) and anionic (OTf^-) components of the ILs. Further, the Ag-[BMIM][OTf] system displayed the highest dipole moment in the gas phase as well as in water. The change in ΔG_f for the formation of Ag-[BMIM][TFSI] was calculated to be the lowest among all three Ag-ILs systems and considered to be the most stable structure. Findings from this study may serve as a fundamental guiding opinion for the design and synthesis of potential pharmaceutical products.

AUTHOR INFORMATION

Corresponding Authors

Lebogang Katata-Seru − *Department of Chemistry, Material Science Innovation & Modelling (MaSIM) Research Focus*

https://doi.org/10.1021/acsomega.3c06171
ACS Omega 2023, 8, 42976−42986

Area, North-West University, Mmabatho 2735, South Africa; Email: lebo.seru@nwu.ac.za

Indra Bahadur − *Department of Chemistry, Material Science Innovation & Modelling (MaSIM) Research Focus Area, North-West University, Mmabatho 2735, South Africa*; orcid.org/0000-0003-2906-473X; Email: bahadur.indra@nwu.ac.za

Authors

Elham Avirdi − *Department of Chemistry, Material Science Innovation & Modelling (MaSIM) Research Focus Area, North-West University, Mmabatho 2735, South Africa*

Hugues Kamdem Paumo − *Department of Chemistry, Material Science Innovation & Modelling (MaSIM) Research Focus Area, North-West University, Mmabatho 2735, South Africa*

Boniface Pone Kamdem − *Laboratory for Phytobiochemistry and Medicinal Plants Study, Department of Biochemistry, Faculty of Science, University of Yaoundé 1, Yaoundé 05508-000, Cameroon*

Madhur Babu Singh − *Department of Chemistry, Atma Ram Sanatan Dharma College, University of Delhi, New Delhi 110021, India*

Kamlesh Kumari − *Department of Zoology, University of Delhi, Delhi 110007, India*

Complete contact information is available at: https://pubs.acs.org/10.1021/acsomega.3c06171

Notes

The authors declare no competing financial interest.

■ ACKNOWLEDGMENTS

E.A. would like to appreciate MaSIM and NWU for all the supports including financial.

■ REFERENCES

(1) Pal, K.; Chakroborty, S.; Nath, N. Limitations of nanomaterials insights in green chemistry sustainable route: Review on novel applications. *Green Process. Synth.* **2022**, *11*, 951−964.

(2) Madani, M.; Hosny, S.; Alshangiti, D. M.; Nadi, N.; Alkhursani, S. A.; Alkhaldi, H.; Al-Gahtany, S. A.; Ghobashy, M. M.; Gaber, G. A. Green synthesis of nanoparticles for varied applications: Green renewable resources and energy-efficient synthetic routes. *Nanotechnol. Rev.* **2022**, *11*, 731−759.

(3) Ssekatawa, K.; Byarugaba, D. K.; Kato, C. D.; Wampande, E. M.; Ejobi, F.; Nakavuma, J. L.; Maaza, M.; Sackey, J.; Nxumalo, E.; Kirabira, J. B. Green strategy−based synthesis of silver nanoparticles for antibacterial applications. *Front. Nanotechnol.* **2021**, *3*, No. 697303.

(4) Ahmed, S.; Ahmad, M.; Swami, B. L.; Ikram, S. A review on plants extract mediated synthesis of silver nanoparticles for antimicrobial applications: A green expertise. *J. Adv. Res.* **2016**, *7*, 17−28.

(5) Giri, A. K.; Jena, B.; Biswal, B.; Pradhan, A. K.; Arakha, M.; Acharya, S.; Acharya, L. Green synthesis and characterization of silver nanoparticles using Eugenia roxburghii DC. extract and activity against biofilm-producing bacteria. *Sci. Rep.* **2022**, *12*, 8383.

(6) Onmaz, N. E.; Yilmaz, D. D.; Imre, K.; Morar, A.; Gungor, C.; Yilmaz, S.; Gundog, D. A.; Dishan, A.; Herman, V.; Gungor, G. Green synthesis of gold nanoflowers using *Rosmarinus officinalis* and *Helichrysum italicum* extracts: Comparative studies of their antimicrobial and antibiofilm activities. *Antibiotics* **2022**, *11*, 1466.

(7) Uhl, B.; Huang, H.; Alwast, D.; Buchner, F.; Behm, R. J. Interaction of ionic liquid with noble metal surfaces: Structure formation and stability of [OMIM][TFSA] and [EMIM][TFSA] on Au(111) and Ag(111). *Phys. Chem. Chem. Phys.* **2015**, *17*, 23816−23832.

(8) Wegner, S.; Janiak, C. Metal nanoparticles in ionic liquids. *Top. Curr. Chem.* **2017**, *375*, 65.

(9) Qamer, S.; Romli, M. H.; Che-Hamzah, F.; Misni, N.; Joseph, N. M. S.; Al-Haj, N. A.; Amin-Nordin, S. Systematic review on biosynthesis of silver nanoparticles and antibacterial activities: Application and theoretical perspectives. *Molecules* **2021**, *26*, 5057.

(10) Bruna, T.; Maldonado-Bravo, F.; Jara, P.; Caro, N. Silver nanoparticles and their antibacterial applications. *Int. J. Mol. Sci.* **2021**, *22*, 7202.

(11) Cui, L.; Chen, P.; Chen, S.; Yuan, Z.; Yu, C.-P.; Ren, B.; Zhang, K. In situ study of the antibacterial activity and mechanism of action of silver nanoparticles by surface-enhanced Raman spectroscopy. *Anal. Chem.* **2013**, *85*, 5436−5443.

(12) Sheng, Z.; Liu, Y. Potential impacts of silver nanoparticles on bacteria in the aquatic environment. *J. Environ. Manage.* **2017**, *191*, 290−296.

(13) Collaborator Antimicrobial Resistance. Global burden of bacterial antimicrobial resistance in A systematic analysis. *Lancet* **2019**, *2022* (399), 629−655.

(14) Gao, W.; Zhang, L. Nanomaterials arising amid antibiotic resistance. *Nat. Rev. Microbiol.* **2021**, *19*, 5−6.

(15) Bélteky, P.; Rónavári, A.; Zakupszky, D.; Boka, E.; Igaz, N.; Szerencsés, B.; Pfeiffer, I.; Vágvölgyi, C.; Kiricsi, M.; Kónya, Z. Are smaller nanoparticles always better? Understanding the biological effect of size-dependent silver nanoparticle aggregation under biorelevant conditions. *Int. J. Nanomed.* **2021**, *16*, 3021−3040.

(16) Javed, R.; Zia, M.; Naz, S.; Aisida, S. O.; Ain, N. U.; Ao, Q. Role of capping agents in the application of nanoparticles in biomedicine and environmental remediation: recent trends and future prospects. *J. Nanobiotechnol.* **2020**, *18*, 172.

(17) Docherty, K. M.; Kulpa, C. F., Jr. Toxicity and antimicrobial activity of imidazolium and pyridinium ionic liquids. *Green Chem.* **2005**, *7*, 185−189.

(18) Maneewattanapinyo, P.; Pichayakorn, W.; Monton, C.; Dangmanee, N.; Wunnakup, T.; Suksaeree, J. Effect of ionic liquid on silver-nanoparticles-complexed Ganoderma applanatum and its topical film formulation. *Pharmaceutics* **2023**, *15*, 1098.

(19) Zhang, P.; Wu, T.; Han, B. Preparation of catalytic materials using ionic liquids as the media and functional components. *Adv. Mater.* **2014**, *26*, 6810−6827.

(20) Patel, R.; Saraswat, J. Effect of imidazolium-based ionic liquid on the antibacterial activity of an expired drug rifampicin. *J. Mol. Liq.* **2021**, *340*, No. 116844.

(21) Siddiquee, M. A.; Saraswat, J.; Imtiyaz, K.; Bhat, A. R.; Wani, F. A.; Alanazi, A. M.; Khan, A. A.; Rizvi, M. M. A.; Patel, R. In-vitro cytotoxicity, synergistic antibacterial activity and interaction studies of imidazolium-based ionic liquids with levofloxacin. *J. Mol. Liq.* **2021**, *325*, No. 115125.

(22) Saraswat, J.; Aldahmash, B.; AlOmar, S. Y.; Imtiyaz, K.; Rizvi, M. M. A.; Patel, R. Synergistic antimicrobial activity of N-methyl substituted pyrrolidinium−based ionic liquids and melittin against Gram-positive and Gram-negative bacteria. *Appl. Microbiol. Biotechnol.* **2020**, *104*, 10465−10479.

(23) Shukla, M.; Verma, A.; Kumar, S.; Pal, S.; Sinha, I. Experimental and DFT calculation study of interaction between silver nanoparticle and 1-butyl-3-methyl imidazolium tetrafluoroborate ionic liquid. *Heliyon* **2021**, *7*, No. e06065.

(24) Avirdi, E.; Paumo, H. K.; Kamdem, B. P.; Singh, M. B.; Kumari, K.; Katata-Seru, L. M.; Bahadur, I. Influence of cation (imidazolium based ionic liquids) as "smart" stabilizers for silver nanoparticles and their evaluation as antibacterial activity on Escherichia coli, Staphylococcus aureus and Enterobacter cloacae. *J. Mol. Liq.* **2023**, *369*, No. 120935.

(25) Jiang, X. C.; Chen, C. Y.; Chen, W. M.; Yu, A. B. Role of citric acid in the formation of silver nanoplates through a synergistic reduction approach. *Langmuir* **2010**, *25*, 4400−4408.

(26) Clinical and Laboratory Standards Institute (CLSI). *Methods for Broth Dilution Susceptibility Testing of Bacteria Isolated From Aquatic Animals*; Approved Guideline. CLSI document M49-A (ISBN 1-56238-612-3) Clinical and Laboratory Standards Institute: 940 West Valley Road, Suite 1400, Wayne, Pennsylvania 19087-1898 USA, 2006.
(27) Li, Z.; Wan, H.; Shi, Y.; Ouyang, P. Personal experience with four kinds of chemical structure drawing software: review on ChemDraw, ChemWindow, ISIS/Draw, and ChemSketch. *J. Chem. Inf. Comput. Sci.* **2004**, *44*, 1886−1890.
(28) Brown, S. A Blended approach to reading and writing graphic stories. *Reading Teach.* **2013**, *67*, 208.
(29) Frisch, M. J.; Trucks, G. W.; Schlegel, H. B.; Scuseria, G. E.; Robb, M. A.; Cheeseman, J. R.; Scalmani, G.; Barone, V.; Petersson, G. A.; Nakatsuji, H.; Li, X.; Caricato, M.; Marenich, A.V.; Bloino, J.; Janesko, B. G.; Gomperts, R.; Mennucci, B.; Hratchian, H. P.; Ortiz, J. V.; Izmaylov, A. F.; Sonnenberg, J. L.; Williams; Ding, F.; Lipparini, F.; Edgidi, F.; Goings, J.; Peng, B.; Petrone, A.; Henderson, T.; Ranasinghe, D.; Zakrzewski, V. G.; Gao, J.; Rega, N.; Zheng, G.; Liang, W.; Hada, M.; Ehara, M.; Toyota, K.; Fukuda, R.; Hasegawa, J.; Ishida, M.; Nakajima, T.; Honda, Y.; Kitao, O.; Nakai, H.; Vreven, T.; Throsell, K.; Montgomery, J. A. Jr.; Peralta, J. E.; Ogliaro, F.; Bearpark, M. J.; Heyd, J. J.; Brothers, E. N.; Kudin, K. N.; Starverov, V. N.; Keith, T. A.; Kobayashi, R.; Normand, J.; Raghavachari, K.; Rendell, A. P.; Burant, J. C.; Iyengar, S. S.; Tomasi, J.; Cossi, M.; Millam, J. M.; Klene, M.; Adamo, C.; Cammi, R.; Ochterski, J. W.; Martin, R. L.; Morokuma, K.; Farkas, O.; Foresman, J. B.; Fox, D. J. *Gaussian 16 Rev. C.01*, 2016.
(30) Frisch, M. J.; Trucks, G. W.; Schlegel, H. E.; Scuseria, G. E.; Robb, M. A.; Cheeseman, J. R.; Scalmani, G.; Barone, V.; Petersson, G. A.; Farkas, O.; Foresman, J. B.; Fox, J. D. *Gaussian 16*, Gaussian, Inc.: Wallingford CT. 2016.
(31) Chiodo, S.; Russo, N.; Sicilia, E. LANL2DZ basis sets recontracted in the framework of density functional theory. *J. Chem. Phys.* **2006**, *125*, No. 104107.
(32) Dennington, R.; Keith, T. A.; Millam, J. M. *GaussView* Version *6*, Semichem Inc. n.d.
(33) Kim, T. Y.; Kim, W. J.; Hong, S. H.; Kim, J. E.; Suh, K. S. Ionic-liquid-assisted formation of silver nanowires. *Angew. Chem., Int. Ed.* **2009**, *48*, 3806−3809.
(34) Liu, H.; Zhang, G.; Lu, L.; Chen, Y.; Luo, M.; Bian, J.; Wang, Z.; Wang, L. Influence of Varied Fluorine Contents on Long-Term Storage Stability of Polyacrylate Nanoparticles and Film Properties. *J. Nanomater.* **2019**, *2019*, No. 2970819.
(35) He, Z.; Alexandridis, P. Nanoparticles in ionic liquids: interactions and organization. *Phys. Chem. Chem. Phys.* **2015**, *17*, 18238−18261.
(36) Weber, H.; Hollóczki, O.; Pensado, A. S.; Kirchner, B. Side chain fluorination and anion effect on the structure of 1-butyl-3-methylimidazolium ionic liquids. *J. Chem. Phys.* **2013**, *139*, No. 084502.
(37) Krajczewski, J.; Kołataj, K.; Kudelski, A. Plasmonic nanoparticles in chemical analysis. *RSC Adv.* **2017**, *7*, 17559−17576.
(38) Roy, K.; Srivastwa, A. K.; Ghosh, C. K. Anticoagulant, thrombolytic and antibacterial activities of *Euphorbia acruensis* latex-mediated bioengineered silver nanoparticles. *Green Process. Synth.* **2019**, *8*, 590−599.
(39) Elmahdy, M. M.; Fahmy, T.; Aldhafeeri, K. A.; Ibnouf, E. O.; Riadi, Y. Optical and antibacterial properties of 1-butyl-3-methyl-imidazolium ionic liquids with trifluoromethanesulfonate or tetra-fluoroborate anion. *Mater. Chem. Phys.* **2021**, *264*, No. 124369.
(40) Ribeiro, M. C. C. Strong anion−anion hydrogen bond in the ionic liquid 1-ethyl-3-methylimidazolium hydrogen sulfate. *J. Mol. Liq.* **2020**, *310*, No. 113178.
(41) Katsyuba, S. A.; Zvereva, E. E.; Yan, N.; Yuan, X.; Kou, Y.; Dyson, P. J. Rationalization of solvation and stabilization of palladium nanoparticles in imidazolium-based ionic liquids by DFT and vibrational spectroscopy. *ChemPhysChem* **2012**, *13*, 1781−1790.
(42) Łuczak, J.; Jungnickel, C.; Łacka, I.; Stolte, S.; Hupka, J. Antimicrobial and surface activity of 1-alkyl-3-methylimidazolium derivatives. *Green Chem.* **2010**, *12*, 593−601.
(43) Fu, F.; Li, Y.; Yang, Z.; Zhou, G.; Huang, Y.; Wan, Z.; Chen, X.-S.; Hu, N.; Li, W.; Huang, L. Molecular-level insights into size-dependent stabilization mechanism of gold nanoparticles in 1-butyl-3-methylimidazolium tetrafluoroborate ionic liquid. *J. Phys. Chem. C* **2017**, *121*, 523−532.
(44) Abbaszadegan, A.; Gholami, A.; Abbaszadegan, S.; Aleyasin, Z. S.; Ghahramani, Y.; Dorostkar, S.; Hemmateenejad, B.; Ghasemi, Y.; Sharghi, H. The effects of different ionic liquid coatings and the length of alkyl chain on antimicrobial and cytotoxic properties of silver nanoparticles. *Iran. Endod. J.* **2017**, *12*, 481−487.
(45) Simões, M.; Rocha, S.; Coimbra, M. A.; Vieira, M. J. Enhancement of *Escherichia coli* and *Staphylococcus aureus* antibiotic susceptibility using sesquiterpenoids. *Med. Chem.* **2008**, *4*, 616−623.
(46) Monte, J.; Abreu, A. C.; Borges, A.; Simões, L. C.; Simões, M. Antimicrobial activity of selected phytochemicals against *Escherichia coli* and *Staphylococcus aureus* and their biofilms. *Pathogens* **2014**, *3*, 473−498.
(47) Ahmad, S. A.; Das, S. S.; Khatoon, A.; Ansari, M. T.; Afzal, M.; Hasnain, M. S.; Nayak, A. K. Bactericidal activity of silver nanoparticles: A mechanistic review. *Mater. Sci. Energy Technol.* **2020**, *3*, 756−769.
(48) More, P. R.; Pandit, S.; Filippis, A.; Franci, G.; Mijakovic, I.; Galdiero, M. Silver nanoparticles: Bactericidal and mechanistic approach against drug resistant pathogens. *Microorganisms* **2023**, *11*, 369.
(49) Duval, R. E.; Gouyau, J.; Lamouroux, E. Limitations of recent studies dealing with the antibacterial properties of silver nanoparticles: fact and opinion. *Nanomaterials* **2019**, *9*, 1775.
(50) Dakal, T. C.; Kumar, A.; Majumdar, R. S.; Yadav, V. Mechanistic basis of antimicrobial actions of silver nanoparticles. *Front Microbiol.* **2016**, *7*, 1831.
(51) Rubim, J. C.; Trindade, F. A.; Gelesky, M. A.; Aroca, R. F.; Dupont, J. Surface-enhanced vibrational spectroscopy of tetrafluoroborate 1-n-butyl-3- methylimidazolium ($BMIBF_4$) ionic liquid on silver surfaces. *J. Phys. Chem. C* **2008**, *112*, 19670−19675.
(52) Ott, L. S.; Cline, M. L.; Deetlefs, M.; Seddon, K. R.; Finke, R. G. Nanoclusters in ionic liquids: evidence for N-heterocyclic carbene formation from imidazolium-based ionic liquids detected by ^2H NMR. *J. Am. Chem. Soc.* **2005**, *127*, 5758−5759.
(53) Ashishie, P. B.; Inah, B. E.; Ayi, A. A. Evaluation of antimicrobial activity of ionic liquid-assisted synthesis of mono-metallic silver and bimetallic copper-silver nanoparticles. *Int. J. Sci.* **2018**, *7*, 25−31.
(54) Singh, M. B.; Kumar, A.; Jain, P.; Singh, P.; Kumari, K. An insight of novel eutectic mixture between thiazolidine-2,4-dione and zinc chloride: Temperature-dependent density functional theory approach. *J. Phys. Org. Chem.* **2021**, *35*, No. e4305.
(55) Singh, M. B.; Jain, P.; Tomar, J.; Kumar, V.; Bahadur, I.; Arya, D. K.; Singh, P. An in silico investigation for acyclovir and its derivatives to fight the COVID-19: Molecular docking, DFT calculations, ADME and td-molecular dynamics simulations. *J. Indian Chem. Soc.* **2022**, *99*, No. 100433.
(56) Kumar, A.; Kumari, K.; Raman, A. P. S.; Jain, P.; Kumar, D.; Singh, P. An insight for the interaction of drugs (acyclovir/ganciclovir) with various ionic liquids: DFT calculations and molecular docking. *J. Phys. Org. Chem.* **2022**, *35*, No. e4287.
(57) Kumar, A.; Kumari, K.; Singh, S.; Bahadur, I.; Singh, P. Noscapine anticancer drug designed with ionic liquids to enhance solubility: DFT and ADME approach. *J. Mol. Liq.* **2021**, *325*, No. 115159.
(58) Marinescu, M.; Cinteză, L. O.; Marton, G. I.; Chifiriuc, M.-C.; Popa, M.; Stănculescu, I.; Zălaru, C.-M.; Stavarache, C.-E. Synthesis, density functional theory study and in vitro antimicrobial evaluation of new benzimidazole Mannich bases. *BMC Chem.* **2020**, *14*, 45.

https://doi.org/10.1021/acsomega.3c06171
ACS Omega 2023, 8, 42976−42986

(59) Xu, Z.; Zhang, C.; Wang, X.; Liu, D. Release strategies of silver ions from materials for bacterial killing. *ACS Appl. Bio Mater.* **2021**, *4*, 3985−3999.

https://doi.org/10.1021/acsomega.3c06171
ACS Omega 2023, 8, 42976−42986